Confronting tridirect *CP*-symmetry models with neutrino oscillation experiments

Gui-Jun Ding,[1,†] Yu-Feng Li,[2,‡] Jian Tang,[3,*] and Tse-Chun Wang[3,§]

[1]*Interdisciplinary Center for Theoretical Study and Department of Modern Physics, University of Science and Technology of China, Hefei, Anhui 230026, China*
[2]*Institute of High Energy Physics, and School of Physical Sciences, University of Chinese Academy of Sciences, Beijing 100049, China*
[3]*School of Physics, Sun Yat-Sen University, Guangzhou 510275, China*

(Received 8 July 2019; published 16 September 2019)

Tridirect *CP* symmetry is an economical neutrino model building paradigm, and it allows for the description of neutrino masses, mixing angles, and *CP* violation phases in terms of four free parameters. The viability of a class of tridirect *CP* models is examined with a comprehensive simulation of current and future neutrino oscillation experiments. The full parameter space of four independent parameters is carefully scanned, and the problem of parameter degeneracy appears for the constraints from one group of neutrino oscillation experiments. Two benchmark models which are promising from a model building point of view are also examined. Complementary roles from accelerator neutrino experiments (e.g., T2HK and DUNE) and reactor neutrino experiments (e.g., JUNO) are crucial to break the degeneracy and nail down the fundamental neutrino mixing parameters of the underlying theory.

DOI: 10.1103/PhysRevD.100.055022

I. INTRODUCTION

Neutrinos in the standard model (SM) of particle physics are strictly massless. Neutrino oscillation requires mass-squared differences and nonzero neutrino masses, which is striking new physics beyond the SM and calls for new degrees of freedom. In the framework of the three-generation neutrino oscillation paradigm, we have two mass-squared differences (Δm^2_{21}, Δm^2_{31}); three mixing angles (θ_{12}, θ_{13}, and θ_{23}); and the Dirac *CP* phase δ_{CP} [1]. The precision of measuring θ_{13} is dominated by reactor neutrino experiments [2–4], θ_{12} and Δm^2_{21} are dominated by the solar and reactor neutrino experiment KamLAND [5–8], and θ_{23} and $|\Delta m^2_{31}|$ are dominated by atmospheric neutrino experiments [4,9,10]. A global analysis of different experiments provides the precise values of mixing parameters at the percentage level [1]. However, the mass ordering $\Delta m^2_{31} > 0$ or $\Delta m^2_{31} < 0$ and the value of δ_{CP} remains unclear, although hints exist from experiments which are currently running.

Many models have been proposed to accommodate massive neutrinos without violating overwhelming constraints from previous experimental results. The origin of neutrino masses, flavor mixing, and *CP* violation is a longstanding open question in particle physics. It turns out that a broken flavor symmetry based on a discrete group is particularly suitable to explain the structure of the leptonic mixing matrix; see Refs. [11–15] for review. If the discrete flavor symmetry is extended to also involve *CP* as a symmetry, the *CP* violation phases in the quark sector (observed) and lepton sector can be predicted [16–18]. Recently a new discrete flavor symmetry model building approach called tridirect *CP* was proposed [19,20], and it is dictated by residual symmetries such that it is quite predictive. The light neutrino mass matrix only depends on four real free parameters to describe the entire neutrino sector (three neutrino masses as well as the lepton mixing matrix). Moreover the *CP* violations in neutrino oscillations and leptogenesis generally arise from the same phase in the tridirect *CP* model; consequently they are closely related to each other.

Precision measurements of neutrino oscillation parameters will guide us to the new physics domain. While in the quark sector, the precision is at the subpercentage level [21], in the neutrino sector, the parameter uncertainties remain at the percentage level [1]. New physics might be hidden in the uncertainties of measured neutrino mixing

*Corresponding author.
tangjian5@mail.sysu.edu.cn
†dinggj@ustc.edu.cn
‡liyufeng@ihep.ac.cn
§wangzejun@mail.sysu.edu.cn

parameters, as neutrino oscillations bridge neutrino mixings and other factors which affect the propagation of coherent states. The new models to accommodate massive neutrinos intend to bring new fundamental symmetries, new particles, and their new interactions beyond the standard model. It is promising to conduct precision measurements in accelerator neutrino experiments to search for new physics, including nonstandard interactions, and neutrino decays (e.g., Refs. [22–32]). It is a question of whether we are able to test different flavor and CP-violation models directly in running accelerator neutrino experiments like T2K [4,33] and NOνA [9,34,35], and future neutrino oscillation experiments like DUNE [36] and T2HK [37]. In this paper, we shall determine the potential of current and upcoming neutrino facilities to test the tridirect CP approach, and the sensitivity regions of oscillation parameters will be presented.

The paper is organized as follows. We first review the tridirect CP symmetry in Sec. II. In Sec. III, we investigate the precision measurements of oscillation parameters, either represented by the standard three-neutrino mixing parameters or denoted by the benchmark model parameters, in running experiments such as T2K and NOνA. We expect better sensitivities in future neutrino experiments, such as T2HK, DUNE, and Jiangmen Underground Neutrino Observatory (JUNO). In Sec. IV, we show our simulation results. We study the precision of model parameters for different experimental configurations and then discuss a degeneracy problem, which can be resolved by including JUNO data. We further study how to constrain oscillation parameters with the restriction of the tridirect CP model, before we discuss two benchmark models. Finally, we summarize our results in Sec. V.

II. REVIEW OF TRIDIRECT CP-SYMMETRY MODELS

Let us firstly recapitulate a benchmark tridirect CP model proposed in [19]. This model is based on the S_4 flavor symmetry and CP symmetry. The flavor group S_4 and CP is broken to the subgroups Z_3^T, $Z_2^{TST^2}\times X_{\mathrm{atm}}$, and $Z_2^U\times X^{\mathrm{sol}}$ in the charged lepton, atmospheric neutrino, and solar neutrino sectors, respectively, where S, T, U are the generators of S_4 and $X_{\mathrm{atm}}=SU$ and $X^{\mathrm{sol}}=U$ denote the residual CP symmetry. In the generic tridirect CP paradigm, the structure of the neutrino and charged lepton mass matrices essentially arise from the vacuum alignment of flavon fields which are fixed by the residual symmetry. In the working basis of [19], the residual flavor symmetry Z_3^T enforces that the charged lepton mass matrix is diagonal [19]. The atmospheric and solar flavon vacuum alignments are determined to be $\langle\phi_{\mathrm{atm}}\rangle\propto(1,\omega^2,\omega)^T$ and $\langle\phi_{\mathrm{sol}}\rangle\propto(1,x,x)^T$, where $\omega=e^{2\pi i/3}$ is a cube root of unity and the parameter x is real because of the imposed CP symmetry. As a result, the Dirac neutrino mass matrix reads as

$$m_D=\begin{pmatrix} y_a & y_s \\ \omega y_a & x y_s \\ \omega^2 y_a & x y_s\end{pmatrix}. \tag{1}$$

The right-handed neutrino Majorana mass matrix is diagonal:

$$m_N=\begin{pmatrix} M_{\mathrm{atm}} & 0 \\ 0 & M_{\mathrm{sol}}\end{pmatrix}. \tag{2}$$

The light effective left-handed Majorana neutrino mass matrix is given by the seesaw formula:

$$m_\nu=m_a\begin{pmatrix} 1 & \omega & \omega^2 \\ \omega & \omega^2 & 1 \\ \omega^2 & 1 & \omega\end{pmatrix}+e^{i\eta}m_s\begin{pmatrix} 1 & x & x \\ x & x^2 & x^2 \\ x & x^2 & x^2\end{pmatrix}, \tag{3}$$

where $m_a=|y_a^2/M_{\mathrm{atm}}|$, $m_s=|y_s^2/M_{\mathrm{sol}}|$, and the only physically important phase η depends on the relative phase between y_a^2/M_{atm} and y_s^2/M_{sol}. It is noteworthy that only four parameters m_a, m_s, η, and x are involved to describe both neutrino masses and lepton mixing parameters. As a consequence, this model is quite predictive. The low-energy phenomenology of this model has been studied both numerically and analytically in [19]. Although x and the relative phase η are free parameters in the general setup of tridirect CP, they can be fixed to some particular values through the vacuum alignment technique in a discrete flavor-symmetry model. It is found that a quite good fit to the experimental data can be obtained for certain choices of x and η; two benchmark examples are $x=-7/2$, $\eta=\pi$ and $x=-4$, $\eta=5\pi/4$. In these benchmark models, the corresponding vacuum alignments take a simple form such that they can be easily realized in concrete models [19,20]. Moreover, the neutrino mass matrix as well as neutrino masses and mixing parameters only depend on two free parameters m_a and m_s in the benchmark models and the experimental data can be accommodated very well.

The neutrino mass spectrum is predicted to be normal ordering in this model, and the lightest neutrino is massless: $m_1=0$. The other two nonvanishing neutrino masses m_2 and m_3 are expressed in terms of the input parameters as follows:

$$m_2^2=\frac{1}{2}[|y|^2+|w|^2+2|z|^2-\sqrt{(|w|^2-|y|^2)^2+4|y^*z+wz^*|^2}],$$
$$m_3^2=\frac{1}{2}[|y|^2+|w|^2+2|z|^2+\sqrt{(|w|^2-|y|^2)^2+4|y^*z+wz^*|^2}], \tag{4}$$

where

$$y=\frac{5x^2+2x+2}{2(x^2+x+1)}(m_a+e^{i\eta}m_s),$$
$$z=-\frac{\sqrt{5x^2+2x+2}}{2(x^2+x+1)}[(x+2)m_a-x(2x+1)e^{i\eta}m_s],$$
$$w=\frac{1}{2(x^2+x+1)}[(x+2)^2m_a+x^2(2x+1)^2e^{i\eta}m_s]. \tag{5}$$

As regards the predictions for lepton flavor mixing, the first column of the mixing matrix is determined to be proportional to $(\sqrt{3}x, \sqrt{x^2+x+1}, \sqrt{x^2+x+1})^T$, the other two columns are uniquely fixed by the input parameters, and the lepton mixing matrix is of the form [19]

$$U=\frac{1}{\sqrt{2}}\begin{pmatrix} \frac{\sqrt{6}x}{\sqrt{5x^2+2x+2}} & 2i\sqrt{\frac{x^2+x+1}{5x^2+2x+2}}\cos\theta & 2i\sqrt{\frac{x^2+x+1}{5x^2+2x+2}}e^{i\psi}\sin\theta \\ \sqrt{\frac{2(x^2+x+1)}{5x^2+2x+2}} & -e^{-i\psi}\sin\theta-\frac{i\sqrt{3}x\cos\theta}{\sqrt{5x^2+2x+2}} & \cos\theta-\frac{i\sqrt{3}xe^{i\psi}\sin\theta}{\sqrt{5x^2+2x+2}} \\ \sqrt{\frac{2(x^2+x+1)}{5x^2+2x+2}} & e^{-i\psi}\sin\theta-\frac{i\sqrt{3}x\cos\theta}{\sqrt{5x^2+2x+2}} & -\cos\theta-\frac{i\sqrt{3}xe^{i\psi}\sin\theta}{\sqrt{5x^2+2x+2}} \end{pmatrix}. \tag{6}$$

The angles θ and ψ are specified by

$$\sin\psi=\frac{\mathcal{J}(y^*z+wz^*)}{|y^*z+wz^*|}, \qquad \cos\psi=\frac{\mathcal{R}(y^*z+wz^*)}{|y^*z+wz^*|},$$
$$\sin 2\theta=\frac{2|y^*z+wz^*|}{\sqrt{(|w|^2-|y|^2)^2+4|y^*z+wz^*|^2}},$$
$$\cos 2\theta=\frac{|w|^2-|y|^2}{\sqrt{(|w|^2-|y|^2)^2+4|y^*z+wz^*|^2}}. \tag{7}$$

As a consequence, we find that the exact expressions for the mixing angles are

$$\sin^2\theta_{13}=\frac{2(x^2+x+1)\sin^2\theta}{5x^2+2x+2},$$
$$\sin^2\theta_{12}=1-\frac{3x^2}{3x^2+2(x^2+x+1)\cos^2\theta},$$
$$\sin^2\theta_{23}=\frac{1}{2}+\frac{x\sqrt{3(5x^2+2x+2)}\sin 2\theta\sin\psi}{2[3x^2+2(x^2+x+1)\cos^2\theta]}. \tag{8}$$

We see that the solar and reactor mixing angles satisfy the following sum rule:

$$\cos^2\theta_{12}\cos^2\theta_{13}=\frac{3x^2}{5x^2+2x+2}. \tag{9}$$

Moreover, from the first column of the mixing matrix in Eq. (6), we can obtain a sum rule for $\cos\delta_{CP}$ in terms of the lepton mixing angles:

$$\cos\delta_{CP}=\frac{\cot 2\theta_{23}[3x^2-(4x^2+x+1)\cos^2\theta_{13}]}{\sqrt{3}|x|\sin\theta_{13}\sqrt{(5x^2+2x+2)\cos^2\theta_{13}-3x^2}}. \tag{10}$$

If the atmospheric mixing angle is maximal, this sum rule implies that the Dirac CP phase would be maximal (i.e., $\delta_{CP}=\pm\pi/2$) as well. Furthermore, the result for the Jarlskog invariant is

$$J_{CP}=\frac{\sqrt{3}x(x^2+x+1)\sin 2\theta\cos\psi}{2(5x^2+2x+2)^{3/2}}, \tag{11}$$

from which we can extract the value of $\sin\delta_{CP}$,

$$\sin\delta_{CP}=\pm\csc 2\theta_{23}\sqrt{1+\frac{(x^2+x+1)^2\cot^2\theta_{13}\cos^2 2\theta_{23}}{3x^2[3x^2\tan^2\theta_{13}-2(x^2+x+1)]}}, \tag{12}$$

with "+" for $x\cos\psi>0$ and "−" for $x\cos\psi<0$. The above results for $\cos\delta_{CP}$ and $\sin\delta_{CP}$ allow us to fix the value of δ_{CP}. Comprehensive numerical analyses show that the allowed region of the parameters x, η, $r=m_a/m_s$, and m_a are $-5.475\leq x\leq -3.370$, $0.455\pi\leq\eta\leq 1.545\pi$, $0.204\leq r\leq 0.606$, and $3.343\text{ meV}\leq m_a\leq 4.597\text{ meV}$ respectively, in order to accommodate the experimental data on neutrino masses and lepton mixing angles [38]. It is remarkable that both the solar mixing angle and Dirac CP phase are predicted to lie in a narrow range $0.329\leq\sin^2\theta_{12}\leq 0.346$ and $1.371\pi\leq\delta_{CP}\leq 1.629\pi$ in this model.

For the benchmark values of the vacuum parameters $x=-7/2$ and $\eta=\pi$, the effective light neutrino mass matrix in Eq. (3) only depends on two free parameters m_a and m_s. Using the general results presented above, we find that the lepton mixing matrix is of the form

$$U = \frac{1}{5\sqrt{6}} \begin{pmatrix} 7\sqrt{2} & -2\sqrt{13}i\cos\theta & 2\sqrt{13}\sin\theta \\ \sqrt{26} & 7i\cos\theta - 5\sqrt{3}\sin\theta & -7\sin\theta + 5\sqrt{3}i\cos\theta \\ \sqrt{26} & 7i\cos\theta + 5\sqrt{3}\sin\theta & -7\sin\theta - 5\sqrt{3}i\cos\theta \end{pmatrix}, \tag{13}$$

where

$$\sin 2\theta = \frac{10|14r-1|}{13\sqrt{4+32r+289r^2}}, \quad \cos 2\theta = \frac{3(8+57r)}{13\sqrt{4+32r+289r^2}}, \tag{14}$$

with $r = m_s/m_a$. The lepton mixing angles read

$$\sin^2\theta_{13} = \frac{26}{75}\sin^2\theta, \qquad \sin^2\theta_{12} = \frac{26\cos^2\theta}{62+13\cos 2\theta}, \quad \sin^2\theta_{23} = \frac{1}{2}, \tag{15}$$

and the Jarlskog invariant is

$$J_{CP} = -\frac{91}{750\sqrt{3}}\sin 2\theta, \tag{16}$$

which implies that the Dirac CP phase is exactly maximal, i.e.,

$$\delta_{CP} = -\pi/2. \tag{17}$$

Notice that both θ_{23} and δ_{CP} are predicted to be maximal and they are favored by the latest data from T2K [39] and NOνA [9,40], the reason is that the neutrino mass matrix of Eq. (3) fulfills the $\mu-\tau$ reflection symmetry in this case. The lightest neutrino masses as functions of m_a and r are

$$m_1^2 = 0, \quad m_2^2 = \frac{9}{8}m_a^2(4-18r+289r^2-|2-17r|\sqrt{4+32r+289r^2}), \quad m_3^2 = \frac{9}{8}m_a^2(4-18r+289r^2+|2-17r|\sqrt{4+32r+289r^2}). \tag{18}$$

In order to accommodate the experimental values of the mixing angles and neutrino mass splittings Δm_{21}^2 and Δm_{31}^2 [38], we find that m_a and r are constrained to lie in rather narrow regions $3.560\,\mathrm{meV} \le m_a \le 3.859\,\mathrm{meV}$ and $0.5282 \le r \le 0.5904$. Accordingly the allowed regions of the reactor and solar mixing angles are strongly constrained: $0.02206 \le \sin^2\theta_{13} \le 0.02349$ and $0.3310 \le \sin^2\theta_{12} \le 0.3319$.

Then we proceed to discuss the second representative values of the vacuum parameters $x = -4$ and $\eta = 5\pi/4$; the lepton mixing matrix reads as

$$U = \frac{1}{\sqrt{74}} \begin{pmatrix} 4\sqrt{3} & -i\sqrt{26}\cos\theta & -i\sqrt{26}e^{i\psi}\sin\theta \\ \sqrt{13} & 2i\sqrt{6}\cos\theta - \sqrt{37}e^{-i\psi}\sin\theta & 2i\sqrt{6}e^{i\psi}\sin\theta + \sqrt{37}\cos\theta \\ \sqrt{13} & 2i\sqrt{6}\cos\theta + \sqrt{37}e^{-i\psi}\sin\theta & 2i\sqrt{6}e^{i\psi}\sin\theta - \sqrt{37}\cos\theta \end{pmatrix}, \tag{19}$$

where a Majorana phase matrix is omitted, and the parameters θ and ψ are functions of the mass ratio r,

$$\tan 2\theta = \frac{2\sqrt{37}\sqrt{4225r^2 + 9(\sqrt{2}-25r+154\sqrt{2}r^2)^2}}{15(-7+3\sqrt{2}r+781r^2)}, \quad \tan\psi = -\frac{65r}{3(\sqrt{2}-25r+154\sqrt{2}r^2)}. \tag{20}$$

The expressions of the mixing angles are

$$\sin^2\theta_{13} = \frac{13}{37}\sin^2\theta, \qquad \sin^2\theta_{12} = \frac{26\cos^2\theta}{61+13\cos 2\theta}, \quad \sin^2\theta_{23} = \frac{1}{2} - \frac{2\sqrt{222}\sin 2\theta\sin\psi}{61+13\cos 2\theta}. \tag{21}$$

The Jarlskog CP invariant takes the form

$$J_{CP} = -\frac{13}{74}\sqrt{\frac{6}{37}}\sin 2\theta\cos\psi. \tag{22}$$

The sum rules for the Dirac CP phase in terms of lepton mixing angles are given by

$$\cos\delta_{CP} = \frac{(35-61\cos 2\theta_{13})\cot 2\theta_{23}}{8\sin\theta_{13}\sqrt{111\cos 2\theta_{13}-33}}, \quad \sin\delta_{CP} = -\csc 2\theta_{23}\sqrt{1-\frac{169\cot^2\theta_{13}\cos^2 2\theta_{23}}{96(13-24\tan^2\theta_{13})}}. \tag{23}$$

It noteworthy that all the lepton mixing angles as well as δ_{CP} only depend on the parameter r through θ and ψ in this case. Moreover, the results for the light neutrino masses are

$$m_1^2 = 0,$$
$$m_2^2 = \frac{1}{2} m_a^2 (9 - 25\sqrt{2} r + 1089 r^2 - \sqrt{81 - 450\sqrt{2}(1 + 121 r^2) r + [(1089 r)^2 - 1052] r^2}),$$
$$m_3^2 = \frac{1}{2} m_a^2 (9 - 25\sqrt{2} r + 1089 r^2 + \sqrt{81 - 450\sqrt{2}(1 + 121 r^2) r + [(1089 r)^2 - 1052] r^2}). \tag{24}$$

In order to describe the experimentally measured values of both lepton mixing angles and neutrino mass-squared differences, we find that the allowed ranges of the input parameters are $3.568\ \mathrm{meV} \le m_a \le 3.871\ \mathrm{meV}$ and $0.3983 \le r \le 0.4473$. As a consequence, the solar and reactor mixing angles are constrained to lie in the narrow intervals $0.02254 \le \sin^2\theta_{13} \le 0.02280$ and $0.3362 \le \sin^2\theta_{12} \le 0.3364$, and the atmospheric mixing angle is predicted to be in the second octant, $0.5559 \le \sin^2\theta_{23} \le 0.5636$. The predicted values of δ_{CP} are distributed around $3\pi/2$, namely, $1.582\pi \le \delta_{CP} \le 1.594\pi$.

Since the model is very predictive and the mixing angles as well as Dirac *CP* phase are constrained to lie in rather narrow regions, in particular we have $0.329 \le \sin^2\theta_{12} \le 0.346$ for the most general case, we expect that the benchmark tridirect model could be excluded in future neutrino experiments. If θ_{23} and δ_{CP} are measured precisely enough, the two values $x = -7/2$, $\eta = \pi$ and $x = -4$, $\eta = 5\pi/4$ may be distinguished from each other. It will be nice to probe these features in detailed simulations of current and future neutrino oscillation experiments.

III. IMPLEMENTATION OF NEUTRINO EXPERIMENTS IN SIMULATION

In this section, we will introduce the current and future experiments: T2K, NOνA, T2HK, DUNE, and JUNO. All sensitivities in experiments are simulated in a state-of-the-art tool GLoBES [41,42] where the experimental details can be very nicely implemented by an abstract experimental design language (AEDL) file. As soon as the publicly available signal and background spectra are reproduced, we can safely claim the expected sensitivities in the precision measurements. In the simulation, input values of neutrino mixing parameters are taken as the best-fit values of the latest NuFit4.0 [1]: $\sin^2\theta_{12} = 0.310$, $\sin^2\theta_{13} = 0.0224$, $\sin^2\theta_{23} = 0.580$, $\delta_{CP} = 215°$, $\Delta m_{21}^2 = 7.39 \times 10^{-5}\ \mathrm{eV}^2$, $\Delta m_{31}^2 = 2.525 \times 10^{-3}\ \mathrm{eV}^2$. In the current study, we will choose a normal mass hierarchy as a demonstration. In the meantime, the preliminary reference Earth model (PREM) density profile is considered in the numerical calculations [43]. We are using two methods to present our results:

(i) Standard three-neutrino oscillations expressed by θ_{12}, θ_{13}, θ_{23}, δ_{CP}, Δm_{21}^2, and Δm_{31}^2 are taken as the truth in nature; we expect that precision measurements of mixing parameters are correlated, and uncertainties of current global fit results are taken into account. For given oscillation parameters, we define a set of parameters:

$$\vec{\mathcal{O}} = \{\theta_{12}, \theta_{13}, \theta_{23}, \delta_{CP}, \Delta m_{21}^2, \Delta m_{31}^2\} \tag{25}$$

and predict the expected event rate in the bin i $\mu_i(\vec{\mathcal{O}})$. We suppose a given experiment reconstructs neutrino spectra in N bins sequentially. The event rate in the bin i is recorded as n_i. We can build a $\chi^2(\vec{\mathcal{O}})$ to quantify the sensitivity:

$$\chi^2(\vec{\mathcal{O}}) = \sum_{i=1}^{N} \frac{[\mu_i(\vec{\mathcal{O}}) - n_i]^2}{\sigma_i^2}. \tag{26}$$

The final results come from a minimization of the summation of the $\chi^2(\vec{\mathcal{O}})$ in every oscillation channel of all experiments over a set of parameters, or the so-called marginalization.

(ii) Once we fit the model parameters, the number of degrees of freedom is reduced from 6 to 4, as shown in the previous section. We consider the following parameters from the tridirect *CP*-symmetry models: x, η, m_a, and r. In this case, we have to change the oscillation parameters predicted by the specific model:

$$\vec{\mathcal{M}} = \{x, \eta, m_a, r\}. \tag{27}$$

Other steps in the likelihood analysis will follow the same strategy as the above method, but replace Eq. (26) by

$$\chi^2(\vec{\mathcal{M}}) = \sum_{i=1}^{N} \frac{[\mu_i(\vec{\mathcal{O}}(\vec{\mathcal{M}})) - n_i]^2}{\sigma_i^2}, \tag{28}$$

with the standard neutrino mixing parameters as functions of model parameters $\vec{\mathcal{O}}(\vec{\mathcal{M}})$. We can expect better measurements of input parameters after a combination of experimental results and symmetry-induced constraints from the theory.

A. T2K

T2K stands for Tokai to Kamioka, a long-baseline experiment in Japan. In Tokai, muon neutrinos or antineutrinos are produced by bombarding a 30 GeV proton beam onto a graphite target station in the J-PARC accelerator center. The neutrino beams are detected first at the near detectors which are 280 m away from the target station. The far detector which reconstructs oscillated neutrino/antineutrino signals is Super-Kamiokande, which has a fiducial mass of 22.5 kt and is 295 km away with an off-axis angle of 2.5° from the beam direction. With the carefully chosen off-axis angle, the neutrino beam energy is peaked at about 0.6 GeV and matches the first maximum in the neutrino oscillation channels: $P(\nu_\mu \to \nu_e)$ and $P(\bar{\nu}_\mu \to \bar{\nu}_e)$.

In 2011, the T2K Collaboration published their first result on $P(\nu_\mu \to \nu_e)$ with 1.43×10^{20} protons on target (POT). It is the first hint of nonzero θ_{13} at the 2.5σ confidence level (C.L.) [33]. In 2012, they presented an analysis of neutrino oscillation for $P(\nu_\mu \to \nu_\mu)$ based on the same POT data, where we have best-fit values of $\Delta m^2_{32} = 2.63 \times 10^{-3}$ eV^2 and $\sin^2 2\theta_{23} = 0.98$ in the three-neutrino mixing framework [44]. In 2016, the first antineutrino result was published based on 4.01×10^{20} POT, where we have best-fit values of $\Delta m^2_{32} = 2.51 \times 10^{-3}$ eV^2 and $\sin^2\theta_{23} = 0.45$. The latest results of searching for *CP* violation in neutrino and antineutrino oscillations by T2K are based on 2.2×10^{21} POT [4]. In our simulation, we equally split 7.8×10^{21} POT into two modes for T2K as the final total POT number.

B. NOνA

NOνA is a long-baseline neutrino oscillation experiment in the United States. Muon neutrinos or antineutrinos are produced by the NuMI beam at Fermilab. The experiment also adopts an off-axis angle of 14.6 mrad to reach the first neutrino oscillation maximum at a peak energy of 2 GeV, since the far detector using 14 kt active scintillator is 810 km away from the target station. The far detector is on the surface. An identical detector with a mass of 290 t scintillator is 100 m deep at a distance of 1 km in order to monitor the neutrino flux and cancel the systematic uncertainties.

In 2016, the NOνA Collaboration published their first result in the $\nu_\mu \to \nu_e$ channel [34] and in the $\nu_\mu \to \nu_\mu$ channel [35] based on 2.74×10^{20} POT. In 2017, they updated results on the electron neutrino appearance channel based on 6.05×10^{20} POT [45]. The degeneracy of θ_{23} shows up at 2.6σ C.L. The latest results in a combination of neutrino and antineutrino runs are given in Ref. [9]. In our simulation, we assume total 36×10^{20} POT for ν and $\bar{\nu}$ modes until 2024 for NOνA.

C. T2HK

An evolution of water Cherenkov detectors from Kamiokande to Hyper-Kamiokande makes it possible to conduct an upgrade of T2K to T2HK [37]. The HyperK detector will have 560 kt fiducial mass to reconstruct neutrino oscillation spectra. T2HK shares the same baseline of 295 km as T2K, while the off-axis beam remains in the same direction with an upgraded proton beam at 1.3 MW. We assume that T2HK will be running in the neutrino mode in 2.5 years and in the antineutrino mode in 7.5 years. The second far detector in Korea is actively under consideration. In our simulation, we will keep the conservative option without the second far detector.

D. DUNE

DUNE is the next-generation accelerator neutrino oscillation experiment with a baseline of 1300 km from FNAL to the underground laboratory in South Dakota. The experiment will search for *CP* violation in the leptonic sector and conduct precision measurements using appearance and disappearance channels by ν_μ and $\bar{\nu}_\mu$ beams. DUNE is going to reconstruct oscillated neutrino spectra with a detector complex of four 10-kt liquid argon time projection chambers (LArTPCs). We adopt an AEDL file provided by Ref. [36]. We assume that the experiment will be running in the neutrino/antineutrino mode in 3.5 years and adopt the three-horn-optimized beam design, which consists of the 62.5 GeV proton beam with a power of 1.83×10^{21} POT per year [46,47].

E. JUNO

JUNO is a multipurpose underground neutrino experiment, which will build a 20 kt liquid scintillator detector in South China and is planned to be online in 2021 [48]. The primary goal of JUNO [49] is to determine the neutrino mass ordering and precision measurement of oscillation parameters using the reactor electron neutrino disappearance channel thanks to the unprecedented energy resolution of $3\%/\sqrt{E}$. Regarding the precision measurement of $|\Delta m^2_{31}|$, Δm^2_{21}, and $\sin^2\theta_{12}$, JUNO can reach the levels of 0.44%, 0.59%, and 0.67%, respectively, after 6 years of data taking. Moreover, the determination of the neutrino mass ordering at reactors is free from the contamination of matter effects [50] and possible new physics [51]. JUNO will be rather robust when combined with accelerator neutrino experiments. The subpercent level precision for three of the six standard oscillation parameters will certainly be powerful for selecting the flavor-symmetry models. In our simulation, we use the standard precision levels as our input priors to combine with accelerator neutrino experiments using the state-of-the-art GLoBES tool.

IV. MODEL TESTING WITH NEUTRINO OSCILLATION EXPERIMENTS

In this section, we show our simulation results with the experiments introduced in Sec. III. The configurations we considered are the synergy of T2K and NOνA, DUNE, T2HK, the combination of all long-baseline (LBL), and the interplay of LBLs and the reactor experiment JUNO. In Sec. IV A, we will first investigate the precision of four model parameters: x, η, r, and m_a. One will see in those results that there is a degeneracy problem. In Sec. IV B, we

TABLE I. The best-fit values of the lepton mixing angles, *CP* violation phases, neutrino masses, and the effective Majorana mass m_{ee} for the benchmark values $(x, \eta) = (-7/2, \pi)$, $(-4, 5\pi/4)$ of the tridirect *CP* model.

x	η	m_a(meV)	r	$\chi^2_{\rm min}$	$\sin^2\theta_{13}$	$\sin^2\theta_{12}$	$\sin^2\theta_{23}$	δ_{CP}/π	β/π	m_2(meV)	m_3(meV)	m_{ee}(meV)
$-\frac{7}{2}$	π	3.716	0.557	17.524	0.0227	0.331	0.5	−0.5	0	8.611	50.232	1.647
−4	$\frac{5\pi}{4}$	3.723	0.421	5.168	0.0226	0.336	0.560	−0.412	0.264	8.603	50.242	2.840

will explain how this degeneracy problem appears and propose a way to resolve this problem. In the following section, we will study how the uncertainties are changed for oscillation parameters by tridirect *CP* models. The above subsections are based on the general tridirect *CP* model. In Table I, we show two benchmark models. Finally, we will predict how these two benchmark models can be tested in future experiments.

A. Precision measurement of model parameters

In Fig. 1, we show the $\Delta\chi^2$ values for each model parameter. We use the true values for the model parameters, $(x, \eta, r, m_a) = (-3.65, 1.1\pi, 0.5, 3.7\ \text{meV})$, which is the best fit for the NuFit4.0 result. We also include the prior according to the NuFit4.0 result. We consider the configurations of DUNE (dashed blue curve), T2HK (dashed green), the combination of NOνA and T2K (dashed brown), the synergy of all LBLs (dashed gray), and the optimized configuration by combining all LBLs and the JUNO experiment (solid red). Except for the m_a result, we see a great improvement in the DUNE result compared to the T2K-and-NOνA combination. T2HK further improves the measurements, and its performance is similar to the combination of all LBLs. This demonstrates the fact that T2HK dominates the contributions. The feature that the performance of T2HK is better than that of DUNE reflects the well-known result that T2HK works better than DUNE with fixed mass ordering, which is naturally imposed by the tridirect *CP* model. In more detail, for x (the upper left panel) the 3σ uncertainty improves from the T2K-and-NOνA combination ($\sim[-4.8, -3.5]$) to DUNE ($\sim[-4.2, -3.5]$) and T2HK ($\sim[-3.8, -3.5]$). The combination of all LBLs performs similarly toT2HK.

Features and tendencies of each $\Delta\chi^2$ curve against r (the lower left panel) are similar to the result for x. The uncertainties at 3σ for the T2K-and-NOνA combination, DUNE, and T2HK are $\sim[0.3, 0.6]$, $\sim[0.4, 0.6]$, and $\sim[0.45, 0.6]$, respectively. The 3σ uncertainty for combining all LBLs is almost the same as that for T2HK. The relative symmetry is seen in the result for η. The sizes of the 3σ uncertainty for the T2K-and-NOνA combination, DUNE, and T2HK are about 0.3π, 0.2π, and 0.15π, respectively. The correlation between η and r worsens

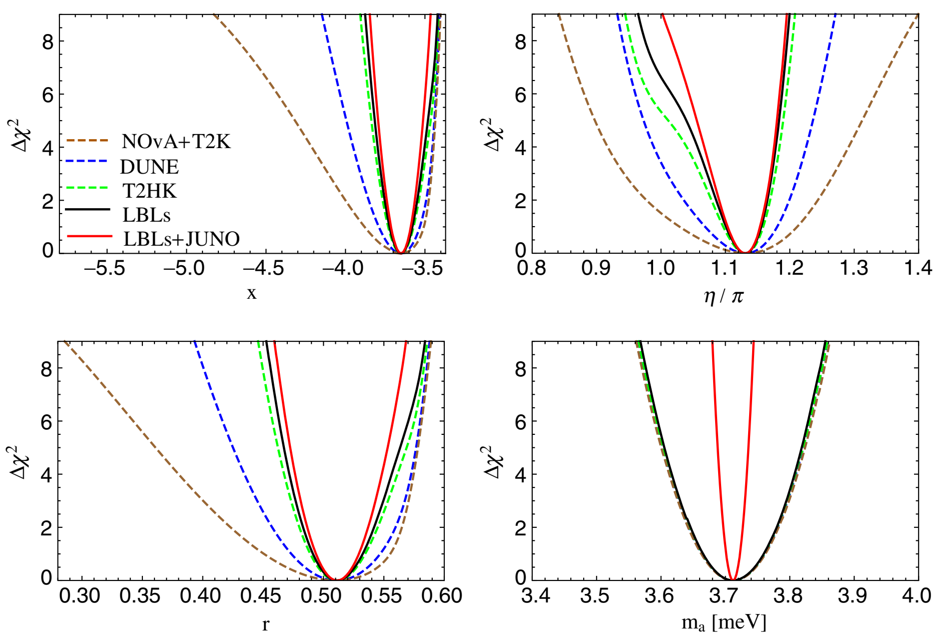

FIG. 1. The $\Delta\chi^2$ value of x, η, r, and m_a in the framework of three-neutrino oscillations taking uncertainties of the NuFit4.0 results. True values for the model parameters are used $(x, \eta, r, m_a) = (-3.65, 1.1\pi, 0.5, 3.7\ \text{meV})$. The experimental configurations we considered are the combination of NOνA and T2K (dashed brown curve); DUNE (dashed blue); T2HK (dashed green); and the combination of all LBLs (solid black), including all LBLs and JUNO (solid red).

the sensitivity for η smaller than the assumed true value. Thanks to the high precision of T2HK and combining all LBLs, the degeneracy problem can be resolved when η is very close to the true value. Therefore, we see a twist around $\eta = \pi$ for these two configurations. Details about this degeneracy will be introduced in Sec. IV B.

For the above three parameters x, η, and r, it is hard to see the improvement by including the data of JUNO to those of all LBLs. Data from JUNO is important for the m_a measurement. We see the overlapping of all curves for all LBL configurations (dashed blue, dashed green, dashed brown, and black curves) in the m_a result. The uncertainty is mainly contributed from Δm^2_{21}, which is not measured well by LBLs. As a result, we see a great improvement by including data from JUNO, which measures Δm^2_{21} well.

We also show the 3σ ($\Delta\chi^2 = 11.83$) contour between any two model parameters in Fig. 2. We see some correlations among x, η, and r for all configurations on $x-\eta$, $x-r$, and $\eta - r$ planes. This correlation is consistent with what we see in Eq. (3), in which m_a is less dependent on the other three parameters. We discover a degeneracy problem related to this correlation for all possible LBL configurations—the combination of NOνA and T2K, DUNE, T2HK, and all-LBL synergy. This degeneracy is mainly caused by the poor measurement of θ_{12}. More details about this degeneracy can be seen in Sec. IV B. These correlations are not removed even if we include JUNO, but combing LBL and JUNO data can resolve the degeneracy problem.

B. Breaking degeneracies

The degeneracy in Fig. 2 can be understood by the equal-oscillation-parameter-value contours on different planes as shown in Fig. 3. In Fig. 3, we show these contours on the $x-\eta$, $x-r$, and $\eta - r$ planes. In the upper panels, we

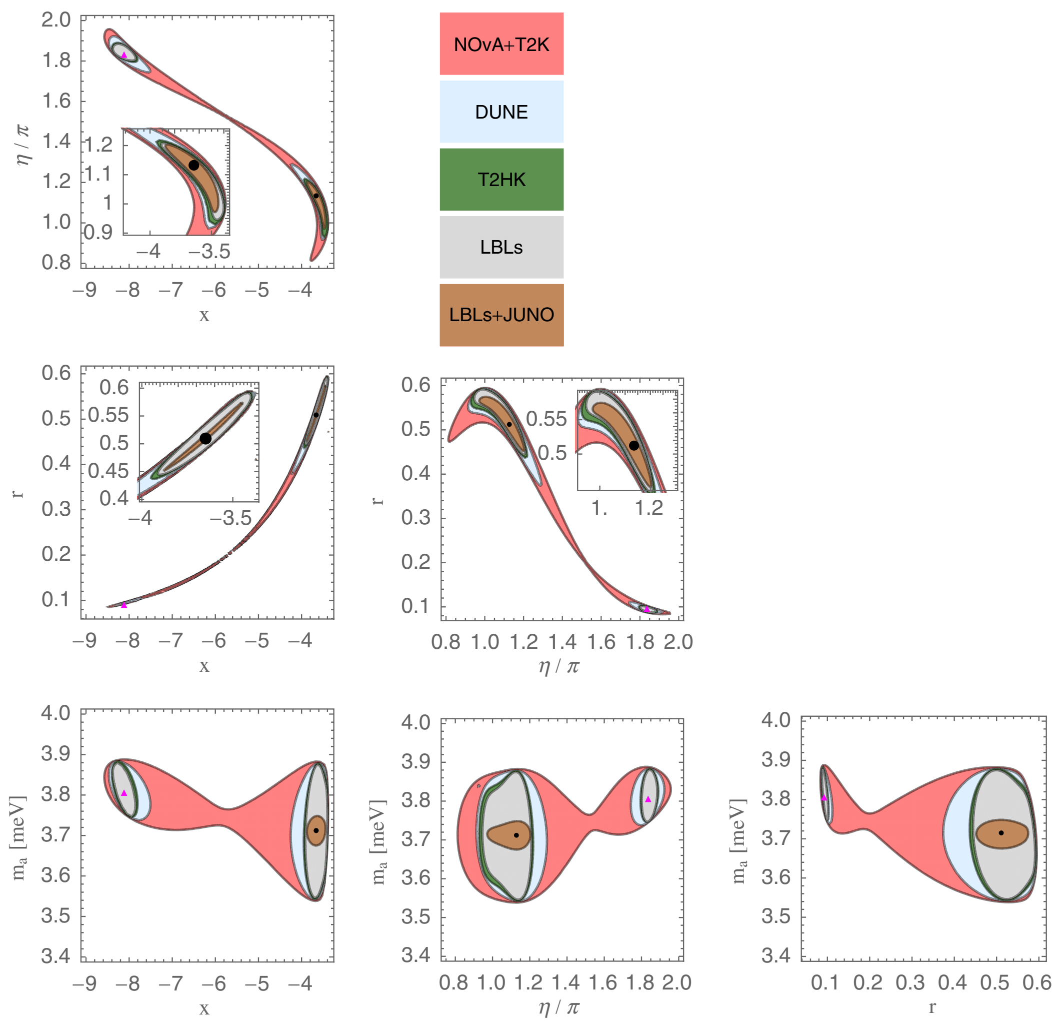

FIG. 2. Precision measurements of any two model parameters at the 3σ confidence level in the framework of three-neutrino oscillations taking uncertainties of the NuFit4.0 results. True values for the model parameters are used: $(x, \eta, r, m_a) = (-3.65, 1.1\pi, 0.5, 3.7\ \text{meV})$. We present the expected results from DUNE (light blue curve), T2HK (green), and the combination NOνA and T2K (pink), as well as the synergy of all LBLs (light gray) and the interplay of LBLs and JUNO (brown). The black dot denotes the best-fit values, while the magenta triangle is for the local minimum, where $r \sim 0.1$, $\eta \sim 1.84\pi$, $x \sim -8$, and $m_a \sim 3.81$ meV.

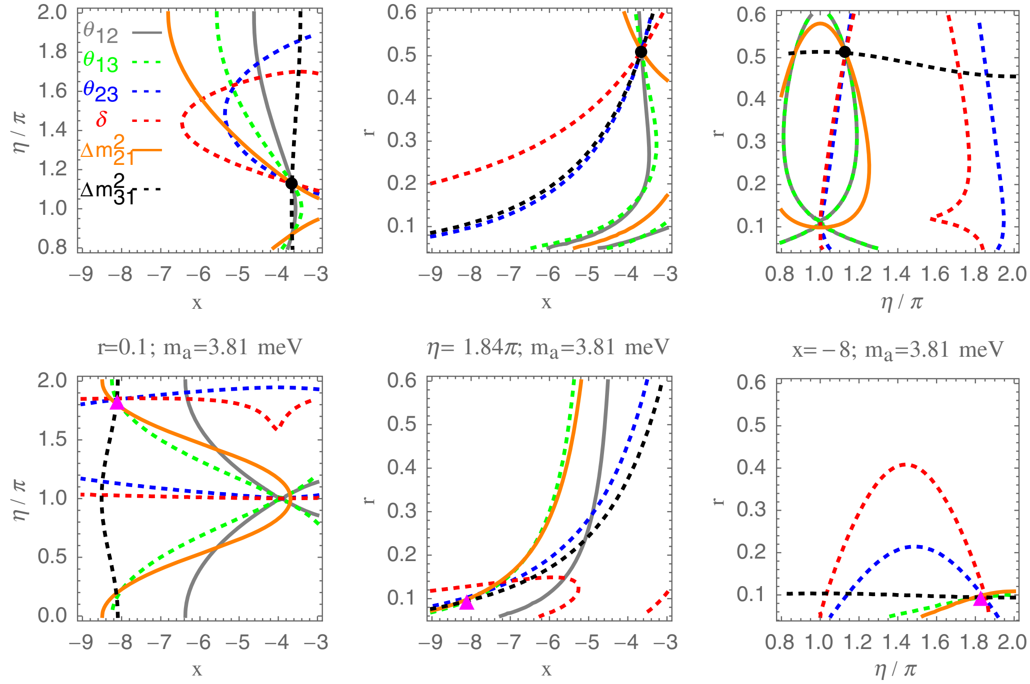

FIG. 3. The contours for $\theta_{12} \sim 35.3°$ (gray), $\theta_{13} \sim 8.6°$ (short-dashed green), $\theta_{23} \sim 47°$ (short-dashed blue), $\delta \sim 279°$ (short-dashed red), $\Delta m^2_{21} \sim 7.4 \times 10^{-5}$ eV^2 (short-dashed orange), and $\Delta m^2_{31} \sim 2.52 \times 10^{-3}$ eV^2 (black) on the $x - \eta$, $x - r$, and $\eta - r$ planes. In the upper panels, we let model parameters be the best-fit values, except for those which are varied. In the lower panels we focus on the degeneracy regions, where $r \sim 0.1$, $\eta \sim 1.84\pi$, $x \sim -8$, and $m_a \sim 3.81$ meV. The gray curve for θ_{12} is below $r = 0.07$ so that it is hardly visible. We show the true values and the local minimum using black dots and magenta triangles, respectively.

set the model parameters at the true values $(x, \eta, r, m_a) = (-3.65, 1.1\pi, 0.5, 3.7 \text{ meV})$, which predicts the value for oscillation parameters $\theta_{12} \sim 35.3°$ (gray curve), $\theta_{13} \sim 8.6°$ (short-dashed green), $\theta_{23} \sim 47°$ (short-dashed blue), $\delta \sim 279°$ (short-dashed red), $\Delta m^2_{21} \sim 7.4 \times 10^{-5}$ eV^2 (orange), and $\Delta m^2_{31} \sim 2.52 \times 10^{-3}$ eV^2 (short-dashed black). The contours are shown with these conditions. Therefore, the intersection of all contours is at the assumed true values. In the lower panels, we focus on the degeneracy region: for the left, middle, and the right panels, we set $r \sim 0.1$, $\eta \sim 1.84\pi$, $x \sim -8$, and $m_a \sim 3.81$ meV. We see that the local minimum of the degeneracy region (magenta triangles) takes place where the green, blue, red, orange, and black curves meet together or go very close. LBL experiments are not sensitive to θ_{12} (gray curve) or Δm^2_{21} (orange curve). As a result, these LBL experiments cannot exclude this region by improving precision. This also explains why once we include reactor data that are sensitive to θ_{12}, the degeneracy region is excluded. One may notice that the different curves do not intersect at the magenta triangle in the $x - r$ plane and there is the gray curve of θ_{12} in the last panel for $\eta - r$. The reason is that the triangle presents a local minimum at which $11.83 > \Delta\chi^2 > 9$. Though that is a local minimum, it does not need to cross all curves. The gray curve of θ_{12} is below $r = 0.07$, where the bottom of the panel is. We did not show it in this panel because the main feature here crossing or going close to θ_{13}, θ_{23}, δ, and Δm^2_{31} results in the degeneracy issue for LBLs.

C. Standard oscillation parameters under tridirect *CP*-symmetry model

In Fig. 4, we show $\Delta\chi^2$ values against all oscillation parameters for the combination of NOνA and T2K (brown curve), DUNE (dashed blue), T2HK (dashed green), the synergy of these four LBLs (gray), and including all LBLs and JUNO (red), assuming the tridirect model. We see that under the tridirect assumption, the combination of NOνA and T2K performs the worst, while DUNE performs much better, except for θ_{13} and Δm^2_{21}. T2HK works slightly better than DUNE and dominates the performance of the combination of all LBLs. The asymmetry for Δm^2_{31} comes from the asymmetry behavior of x and r in Fig. 1 through Eq. (4). Obviously, the twist behavior for η is passed to those for θ_{13}, θ_{23}, and δ by the tridirect model. We note that even LBL experiments are not sensitive to θ_{12}; the uncertainty can be improved by precisely measuring other oscillation parameters within the tridirect model. We further point out a great improvement by including JUNO data which can be seen in the result for Δm^2_{21}.

In Fig. 5, we show the points at the 3σ surface projected on θ_{23}-Δm^2_{31} (upper left), θ_{13}-Δm^2_{31} (upper right), θ_{12}-Δm^2_{21} (lower left), and θ_{13}-δ (lower right) for the synergy of these four LBLs (gray curve) and including all LBLs and JUNO (red). Because of the nonlinear relations between model parameters and standard parameters, the data do not spread uniformly. We also compare them with those without the

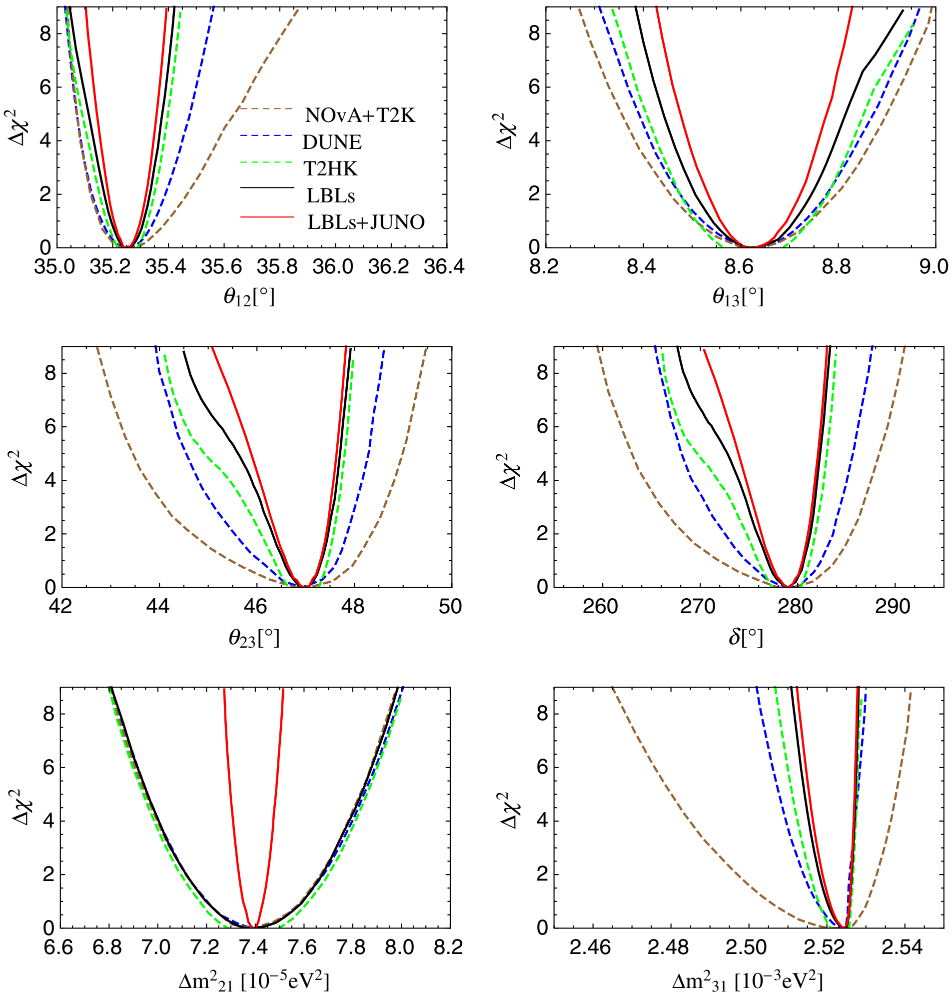

FIG. 4. The $\Delta\chi^2$ value against θ_{12} (upper left), θ_{13} (upper right), θ_{23} (middle left), δ (middle right), Δm^2_{21} (lower left), and Δm^2_{31} (lower right), for DUNE (dashed blue curve), T2HK (dashed green), the combination of NOνA and T2K (dashed brown), the synergy of these four LBLs (black), and including all LBLs and JUNO (red), assuming the tridirect *CP* model.

restriction from the tridirect *CP* model: the gray curve is for including all LBLs, while the dashed black curve is for a combination of LBLs and JUNO. There is a discontinuity when θ_{13} is larger than $\sim 8.8°$, because of the degeneracy with θ_{23}. These results show that assuming tridirect *CP* improves the key measurements for future experiments.

D. A discrimination of two benchmark models

In Fig. 6, we show $\Delta\chi^2$ against r (left) and m_a (right) assuming model A [solid curve; Eq. (13)] and model B [dotted curve; Eq. (19)], for DUNE (blue curve), T2HK (green), the combination of NOνA and T2K (brown), the synergy of four LBLs (black), and the interplay of LBL and JUNO data (red). These two models, shown in Table I, assume different values for x and η: $(x, \eta) = (-7/2, \pi)$ for model A and $(x, \eta) = (-4, 5\pi/4)$ for model B. The corresponding best fits with the global fit result are given $(r, m_a) = (0.557, 3.716\ \text{meV})$ for model A and $(r, m_a) = (0.421, 3.723\ \text{meV})$ for model B. We see that based on one model, the better way to exclude the other one is by precision measurement of r. The experimental configuration does not affect the uncertainty for r. This uncertainty is ~ 0.2 at 3σ under both models. Two models predict very similar values for m_a. As a result, it is impossible to exclude the wrong model by measuring this parameter alone. Moreover, the uncertainty of m_a depends on the model and the experimental configuration. The precision under model A is generally better than that for model B, except for the combination of LBL and JUNO data. The rank of precision from the worst to the best experimental configuration is the combination of NOνA and T2K, DUNE, T2HK, the synergy of all LBLs, and combining all LBLs and JUNO. Both m_a and m_s will be determined precisely by experiments. As given in the definition, the model discriminator $r \equiv m_a/m_s$ points to a requirement to measure both mass-squared differences in neutrino experiments as precisely as possible.

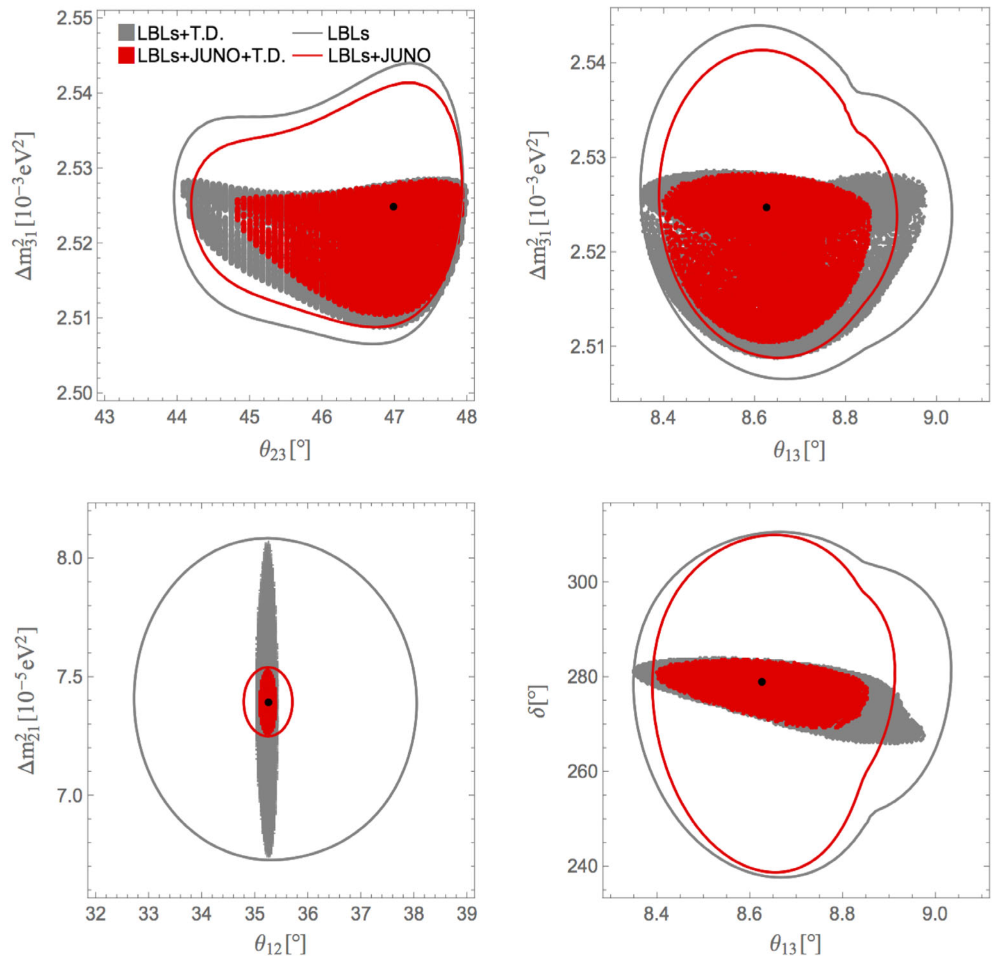

FIG. 5. The points on the 3σ sphere in the four-dimensional model-parameter space projected on θ_{23}-Δm^2_{31} (upper left), θ_{13}-Δm^2_{31} (upper right), θ_{12}-Δm^2_{21} (lower left), and θ_{13}-δ (lower right) for the synergy of these four LBLs (gray curve) and including all LBLs and JUNO (red). We also compare these results to those without the restrictions from tridirect models for LBL synergy (gray contour) and combing all experiments (red contour).

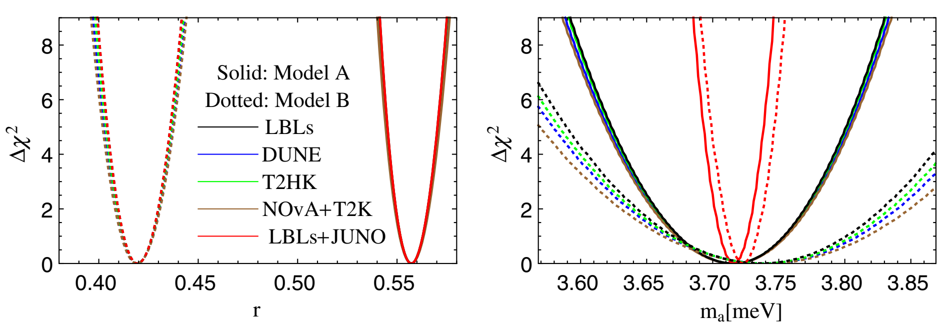

FIG. 6. The $\Delta\chi^2$ value against r (left) and m_a (right) assuming model A [solid curve; Eq. (13)] and model B [dotted curve; Eq. (19)], for DUNE (blue), T2HK (green), the combination of NOνA and T2K (brown), the synergy of four LBLs (black), and the interplay of LBLs and JUNO (red). In model A (B), two conditions are assumed: $x = -7/2$ and $\eta = \pi$ ($x = -4$ and $\eta = 5\pi/4$), while in the current global fit results the best fits for the other two parameters are located at $(r, m_a) = (0.557, 3.716\ \text{meV})$ [$(r, m_a) = (0.421, 3.723\ \text{meV})$].

V. SUMMARY

The tridirect *CP*-symmetry model offers fruitful features to accommodate neutrino masses and explain neutrino mixing and oscillations. The more powerful aspect is the model predicted correlations of standard neutrino mixing parameters preserved by an underlying symmetry. We looked into a probe of the tridirect *CP*-symmetry model by simulating the current and future neutrino oscillation experiments, including T2K, NOνA, T2HK, DUNE, and JUNO. We found that the degeneracy problem cannot be avoided at a single long-baseline experiment in the precision measurement of model parameters while a combination of long-baseline and reactor experiments will resolve the problem. This fact highlights the complementarity of different neutrino oscillation experiments. In addition, we scanned the standard neutrino mixing parameters expressed by the underlying model "true" values in order to determine how powerful precision measurements in the traditional analysis will be. It seems that the shapes of contours in the projected parameter space can give us hints of the underlying theory but the information remains limited by a multiple-channel analysis in a single experiment. This limitation points to a combined analysis by multiple experiments with different beams and baseline configurations. Finally, we can discriminate among benchmark models after a discovery of *CP* violation in the leptonic sector by any one of these experiments.

ACKNOWLEDGMENTS

This work is supported in part by the National Natural Science Foundation of China under Grants No. 11505301, No. 11881240247, No. 11522546, and No. 11835013. J. T. appreciates ICTP's hospitality and nice discussions with participants during the workshop PANE2018. The work was initiated and expanded at the Chinese High-Energy Physics Conference and the MOMENT&EMuS meeting. We also thank Dr. Nick W. Prouse to kindly provide the simulation package for T2HK. Finally, we appreciate Dr. Neil Drouard Raper's help to improve the readability of our paper.

APPENDIX: PHYSICS PERFORMANCE OF DIFFERENT CONFIGURATIONS

In this section, we demonstrate the experimental potential for different configurations by showing the 1σ, 2σ, and 3σ contours on the θ_{23}-δ and θ_{23}-Δm^2_{31} planes. These measurements are the main goals for current and future LBLs. For current running experiments NOνA (upper) and

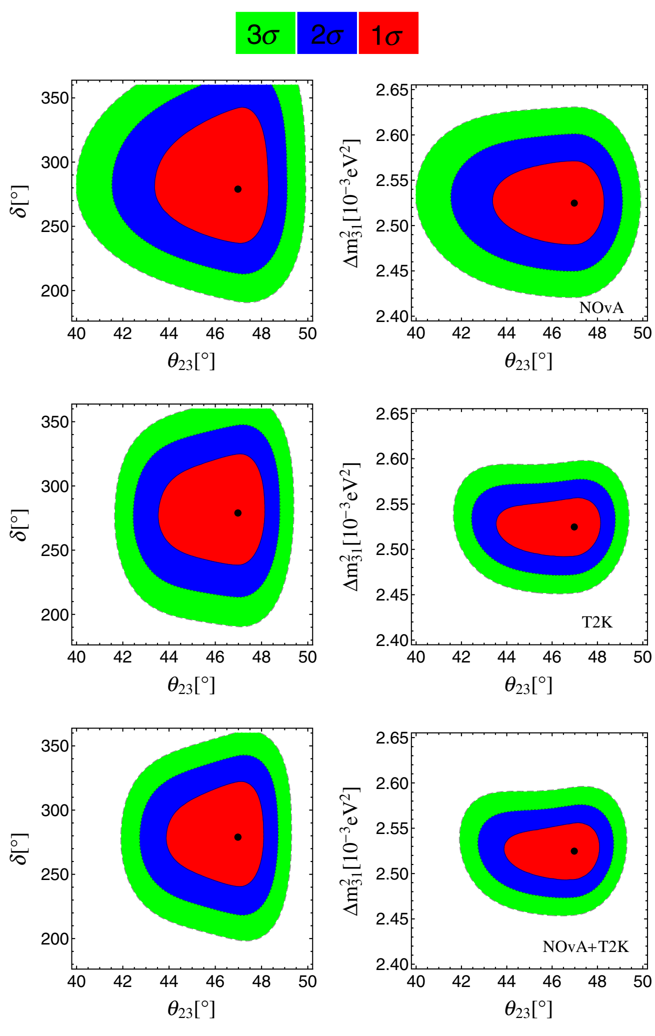

FIG. 7. The contours on θ_{23}-δ (left) and θ_{23}-Δm^2_{31} (right) for NOνA (upper) planes, T2K (middle), and their combination (lower) at 1σ (red curve), 2σ (blue), and 3σ (green) precision. The true values are $\theta_{12} \sim 35.3°$, $\theta_{13} \sim 8.6°$, $\theta_{23} \sim 47°$, $\delta \sim 279°$, $\Delta m^2_{21} \sim 7.4 \times 10^{-5}$ eV^2, and $\Delta m^2_{31} \sim 2.52 \times 10^{-3}$ eV^2. These results include the NuFit4.0 results as priors.

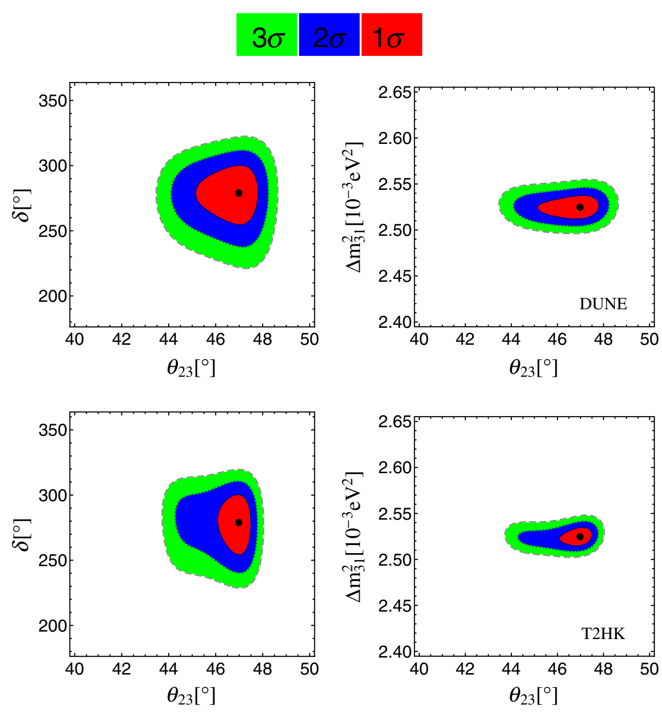

FIG. 8. The contours on θ_{23}-δ (left) and θ_{23}-Δm^2_{31} (right) for DUNE (upper) and T2HK (lower) at 1σ (red curve), 2σ (blue), and 3σ (green) precision. The true values are $\theta_{12} \sim 35.3°$, $\theta_{13} \sim 8.6°$, $\theta_{23} \sim 47°$, $\delta \sim 279°$, $\Delta m^2_{21} \sim 7.4 \times 10^{-5}$ eV^2, and $\Delta m^2_{31} \sim 2.52 \times 10^{-3}$ eV^2. These results include the NuFit4.0 results as priors.

T2K (middle), we show their expected final performance in Fig. 7. For NOνA, we assume total 36×10^{20} POT for ν and $\bar{\nu}$ modes until 2024, while for T2K we equally split 7.8×10^{21} POT into two modes. We also show the combination of these two experiments in the lower panels of Fig. 7. In Fig. 8, we show the performance of DUNE (upper) and T2HK (lower). For DUNE, we consider the three-horn-optimized design with 1.83×10^{21} POT per year, and we adopt 3.5 years for each mode. For T2HK, we assume a 1.3 MW proton beam for the neutrino source, and run ν and $\bar{\nu}$ modes for 2.5 and 7.5 years, respectively. More details about these experiments can be seen in Sec. III.

[1] I. Esteban, M. C. Gonzalez-Garcia, A. Hernandez-Cabezudo, M. Maltoni, and T. Schwetz, Global analysis of three-flavour neutrino oscillations: Synergies and tensions in the determination of θ_23, δ_CP, and the mass ordering, J. High Energy Phys. 01 (2019) 106.

[2] D. Adey *et al.* (Daya Bay Collaboration), Measurement of the Electron Antineutrino Oscillation with 1958 Days of Operation at Daya Bay, Phys. Rev. Lett. **121**, 241805 (2018).

[3] H. De Kerret *et al.* (Double Chooz Collaboration), First Double Chooz θ_{13} Measurement via Total Neutron Capture Detection, arXiv:1901.09445.

[4] K. Abe *et al.* (T2K Collaboration), Search for *CP* Violation in Neutrino and Antineutrino Oscillations by the T2K Experiment with 2.2×10^{21} Protons on Target, Phys. Rev. Lett. **121**, 171802 (2018).

[5] B. T. Cleveland, T. Daily, R. Davis, Jr., J. R. Distel, K. Lande, C. K. Lee, P. S. Wildenhain, and J. Ullman, Measurement of the solar electron neutrino flux with the Homestake chlorine detector, Astrophys. J. **496**, 505 (1998).

[6] K. Abe *et al.* (Super-Kamiokande Collaboration), Solar neutrino results in Super-Kamiokande-III, Phys. Rev. D **83**, 052010 (2011).

[7] B. Aharmim *et al.* (SNO Collaboration), Combined analysis of all three phases of solar neutrino data from the Sudbury neutrino observatory, Phys. Rev. C **88**, 025501 (2013).

[8] C. Ghiano (Borexino Collaboration), Solar neutrino results and future opportunities with Borexino, J. Phys. Conf. Ser. **1137**, 012054 (2019).

[9] M. A. Acero *et al.* (NOνA Collaboration), New constraints on oscillation parameters from ν_e appearance and ν_μ disappearance in the NOνA experiment, Phys. Rev. D **98**, 032012 (2018).

[10] P. Adamson *et al.* (MINOS Collaboration), Electron Neutrino and Antineutrino Appearance in the Full MINOS Data Sample, Phys. Rev. Lett. **110**, 171801 (2013).

[11] G. Altarelli and F. Feruglio, Discrete flavor symmetries and models of neutrino mixing, Rev. Mod. Phys. **82**, 2701 (2010).

[12] H. Ishimori, T. Kobayashi, H. Ohki, Y. Shimizu, H. Okada, and M. Tanimoto, Non-Abelian discrete symmetries in particle physics, Prog. Theor. Phys. Suppl. **183**, 1 (2010).

[13] S. F. King and C. Luhn, Neutrino mass and mixing with discrete symmetry, Rep. Prog. Phys. **76**, 056201 (2013).

[14] S. F. King, A. Merle, S. Morisi, Y. Shimizu, and M. Tanimoto, Neutrino mass and mixing: From theory to experiment, New J. Phys. **16**, 045018 (2014).

[15] S. F. King, Models of neutrino mass, mixing and CP violation, J. Phys. G **42**, 123001 (2015).

[16] C.-C. Li, J.-N. Lu, and G.-J. Ding, Toward a unified interpretation of quark and lepton mixing from flavor and *CP* symmetries, J. High Energy Phys. 02 (2018) 038.

[17] J.-N. Lu and G.-J. Ding, Quark and lepton mixing patterns from a common discrete flavor symmetry with a generalized *CP* symmetry, Phys. Rev. D **98**, 055011 (2018).

[18] J.-N. Lu and G.-J. Ding, Dihedral flavor group as the key to understand quark and lepton flavor mixing, J. High Energy Phys. 03 (2019) 056,

[19] G.-J. Ding, S. F. King, and C.-C. Li, Tri-direct *CP* in the littlest seesaw playground, J. High Energy Phys. 12 (2018) 003.

[20] G.-J. Ding, S. F. King, and C.-C. Li, Lepton mixing predictions from S_4 in the tridirect *CP* approach to two right-handed neutrino models, Phys. Rev. D **99**, 075035 (2019).

[21] M. Tanabashi *et al.* (Particle Data Group Collaboration), Review of particle physics, Phys. Rev. D **98**, 030001 (2018).

[22] T. Wang and Y.-L. Zhou, Neutrino nonstandard interactions as a portal to test flavor symmetries, Phys. Rev. D **99**, 035039 (2019).

[23] I. Esteban, M. C. Gonzalez-Garcia, M. Maltoni, I. Martinez-Soler, and J. Salvado, Updated constraints on non-standard interactions from global analysis of oscillation data, J. High Energy Phys. 08 (2018) 180.

[24] J. Tang, Y. Zhang, and Y.-F. Li, Probing direct and indirect unitarity violation in future accelerator neutrino facilities, Phys. Lett. B **774**, 217 (2017).

[25] J. Tang and Y. Zhang, Study of nonstandard charged-current interactions at the MOMENT experiment, Phys. Rev. D **97**, 035018 (2018).

[26] M. V. Ascencio-Sosa, A. M. Calatayud-Cadenillas, A. M. Gago, and J. Jones-Pérez, Matter effects in neutrino visible decay at future long-baseline experiments, Eur. Phys. J. C **78**, 809 (2018).

[27] J. Tang, T.-C. Wang, and Y. Zhang, Invisible neutrino decays at the MOMENT experiment, J. High Energy Phys. 04 (2019) 004.

[28] P. Coloma, Non-standard interactions in propagation at the Deep Underground Neutrino Experiment, J. High Energy Phys. 03 (2016) 016.

[29] J. Liao, D. Marfatia, and K. Whisnant, Nonstandard neutrino interactions at DUNE, T2HK and T2HKK, J. High Energy Phys. 01 (2017) 071.

[30] M. Masud, M. Bishai, and P. Mehta, Extricating new physics scenarios at DUNE with higher energy beams, Sci. Rep. **9**, 352 (2019).

[31] N. D. Kuchibhatla, S. Goswami, and N. Nath, Effect of non-standard neutrino interactions on the sensitivities of DUNE, Proc. Sci., NuFact2017 (**2018**) 162.

[32] K. N. Deepthi, S. Goswami, and N. Nath, Challenges posed by non-standard neutrino interactions in the determination of δ_{CP} at DUNE, Nucl. Phys. **B936**, 91 (2018).

[33] K. Abe *et al.* (T2K Collaboration), Indication of Electron Neutrino Appearance from an Accelerator-Produced Off-Axis Muon Neutrino Beam, Phys. Rev. Lett. **107**, 041801 (2011).

[34] P. Adamson *et al.* (NOνA Collaboration), First Measurement of Electron Neutrino Appearance in NOνA, Phys. Rev. Lett. **116**, 151806 (2016).

[35] P. Adamson *et al.* (NOνA Collaboration), First measurement of muon-neutrino disappearance in NOνA, Phys. Rev. D **93**, 051104 (2016).

[36] T. Alion *et al.* (DUNE Collaboration), Experiment simulation configurations used in DUNE CDR, arXiv:1606.09550.

[37] K. Abe *et al.* (Hyper-Kamiokande Collaboration), Hyper-Kamiokande Design Report, arXiv:1805.04163.

[38] I. Esteban, M. C. Gonzalez-Garcia, M. Maltoni, I. Martinez-Soler, and T. Schwetz, Updated fit to three neutrino mixing: Exploring the accelerator-reactor complementarity, J. High Energy Phys. 01 (2017) 087.

[39] K. Abe *et al.* (T2K Collaboration), Combined Analysis of Neutrino and Antineutrino Oscillations at T2K, Phys. Rev. Lett. **118**, 151801 (2017).

[40] P. Adamson *et al.* (NOνA Collaboration), Constraints on Oscillation Parameters from ν_e Appearance and ν_μ Disappearance in NOνA, Phys. Rev. Lett. **118**, 231801 (2017).

[41] P. Huber, M. Lindner, and W. Winter, Simulation of long-baseline neutrino oscillation experiments with GLoBES (General Long Baseline Experiment Simulator), Comput. Phys. Commun. **167**, 195 (2005).

[42] P. Huber, J. Kopp, M. Lindner, M. Rolinec, and W. Winter, New features in the simulation of neutrino oscillation experiments with GLoBES 3.0: General Long Baseline Experiment Simulator, Comput. Phys. Commun. **177**, 432 (2007).

[43] A. M. Dziewonski and D. L. Anderson, Preliminary reference Earth model, Phys. Earth Planet. Inter. **25**, 297 (1981).

[44] K. Abe *et al.* (T2K Collaboration), Measurement of Muon Antineutrino Oscillations with an Accelerator-Produced Off-Axis Beam, Phys. Rev. Lett. **116**, 181801 (2016).

[45] P. Adamson *et al.* (NOνA Collaboration), Measurement of the Neutrino Mixing Angle θ_{23} in NOνA, Phys. Rev. Lett. **118**, 151802 (2017).

[46] V. Papadimitriou *et al.*, Design of the LBNF Beamline, in *Proceedings, 7th International Particle Accelerator Conference (IPAC 2016): Busan, Korea, 2016* (JACoW, Geneva, 2016), p. TUPMR025, https://doi.org/10.18429/JACoW-IPAC2016-TUPMR025.

[47] S. Tariq *et al.* (LBNF Collaboration), Design of the LBNF Beamline Target Station, in *Proceedings, 2nd North American Particle Accelerator Conference (NAPAC2016): Chicago, Illinois, USA, 2016* (JACoW, Geneva, 2017), p. MOPOB35, https://doi.org/10.18429/JACoW-NAPAC2016-MOPOB35.

[48] Z. Djurcic *et al.* (JUNO Collaboration), JUNO Conceptual Design Report, arXiv:1508.07166.

[49] F. An *et al.* (JUNO Collaboration), Neutrino physics with JUNO, J. Phys. G **43**, 030401 (2016).

[50] Y.-F. Li, Y. Wang, and Z.-z. Xing, Terrestrial matter effects on reactor antineutrino oscillations at JUNO or RENO-50: How small is small?, Chin. Phys. C **40**, 091001 (2016).

[51] Y.-F. Li, Z.-z. Xing, and J.-y. Zhu, Indirect unitarity violation entangled with matter effects in reactor antineutrino oscillations, Phys. Lett. B **782**, 578 (2018).